

4<sup>th</sup> IAA Planetary Defense Conference – PDC 2015  
13-17 April 2015, Frascati, Roma, Italy

IAA-PDC-15-03-12

## ASTEROID DEFENSE: COMPARISON OF KINETIC-IMPACT AND NUCLEAR STAND-OFF SCHEMES

Galen R. Gisler<sup>(1,2)</sup>, Jim M. Ferguson<sup>(1)</sup>, Catherine S. Plesko<sup>(1)</sup>  
and Robert P. Weaver<sup>(1)</sup>

<sup>(1)</sup>Los Alamos National Laboratory, MS P365, Los Alamos NM 87544 USA,  
+1 505 920 2722, [galengisler@mac.com](mailto:galengisler@mac.com)

<sup>(2)</sup>Department of Mathematics, University of Oslo, Blindern 0316 Oslo, Norway

**Keywords:** *asteroid deflection techniques, hydrocode simulations, momentum amplification, kinetic impactor, nuclear stand-off burst*

### ABSTRACT

In this work we study the deflection of hazardous near-earth objects using either a kinetic impactor or a nuclear stand-off burst. If the object is known to be competent, the kinetic impactor is shown to be highly efficient. The momentum delivered to the object can be much greater than the momentum of the impactor because of the reaction force produced by ablation from the impact crater. We use an adaptive-mesh hydrocode to study the achieved push velocity and momentum-enhancement factor, or beta, varying the target diameter, target porosity, and velocity of the impactor. Spall from the back side of the asteroid, which partly counters the favorable effect of ablation, is also included in the calculations. For objects not known to be competent, the nuclear stand-off burst option may be preferable. In this case, crucial questions surround the optimum height of burst and the radiation characteristics of the burst. The same hydrocode, with radiation diffusion included, is used to study this case as well. Figures of merit from both these studies include the bulk momentum imparted to the asteroid and the degree to which the asteroid is disrupted.

### 1. Kinetic Impact

**Scenario:** We imagine a spacecraft sent to intercept a threatening near-earth asteroid. Upon close approach, the spacecraft fires a projectile at the asteroid, such that the spacecraft's velocity combined with that of the projectile is sufficient to excavate a crater and impart a substantial momentum boost. The spacecraft itself flies past the asteroid while its sensors record the result of the impact. A design for such a mission is given, for example, in [1].

In general, the momentum delivered to the asteroid will be greater than the momentum of the impacting projectile because of ejecta from the crater. The ejected material moves back at high speed in the direction from which the projectile came. This ablated material provides an additional momentum boost to the asteroid, according to Newton's third law of motion. It is conventional to express this boost as

a momentum multiplication factor,  $\beta$ , formulated as the ratio of the asteroid momentum after collision ( $p_{\text{push}}$ ) to the projectile momentum before collision ( $p_{\text{projectile}}$ ) [2]:

$$\beta_{\text{kinetic}} = \frac{P_{\text{push}}}{P_{\text{projectile}}} \quad (1)$$

A critical research focus in kinetic energy deflection lies in determining what values of  $\beta$  are possible or likely for given scenarios.

**What determines  $\beta$ ?** The additional thrust given to the asteroid depends on the speed and mass of the material ejected from the crater, and these quantities are in turn dependent upon the material composition, porosity, and strength of the asteroid material. For most, if not all, asteroids, these are unknown. Some general remarks can be made, however. If the material of the asteroid's crust is rich in volatiles,  $\beta$  should be higher than if not. If the material has very high strength,  $\beta$  should be lower, because less material would be ablated from the crater on the frontside, and some material would be spalled from the backside. The porosity of the asteroid will affect  $\beta$  since the shock passing through the asteroid must expend some energy in crushing out the pores. Hence  $\beta$  will be higher for nonporous bodies than for highly porous ones. Of course, the kinetic energy of the impacting projectile will also affect  $\beta$ .

**The calculations.** We have performed a series of calculations to study the dependence of  $\beta$  on the kinetic energy and composition of the projectile and on the composition and porosity of the asteroid. For the asteroid we have used two compositions, namely basalt and alluvium, both dry (*i.e.* no volatiles), with equations of state from the LANL SESAME tables. We have used both Steinberg-Guinan and Wilkins-Gittings strength models, with very low strength, and see no substantial differences between these two models. By adjusting the asteroid porosity from zero to 60%, we have target densities ranging from 2.9 g/cm<sup>3</sup> (zero-porosity basalt) down to 1.0 g/cm<sup>3</sup> (60% porosity alluvium). Our asteroid targets were uniform-density spheres of diameters 100, 300, and 500 m, the latter being an approximate match to 101955 Bennu, the target for the OSIRIS/REx mission.

The impact is designed to occur on-axis, so that two-dimensional calculations are sufficient. We used three impact velocities (10, 15, and 20 km/s), and two projectile compositions, namely an iron sphere of 64 cm diameter and an aluminum sphere of 92 cm diameter, both of a little more than 1 metric ton mass. The iron and aluminum equations of state are also from the LANL SESAME tables. The kinetic energy delivered to the asteroid ranged from 0.013 to 0.053 kiloton TNT equivalent.

The code used for these calculations is RAGE, an adaptive-mesh-refinement hydrocode originally developed at Science Applications International and subsequently modified at Los Alamos National Laboratory. RAGE is a multi-material code well suited to problems of this nature [3].

The initial configuration for a typical calculation is illustrated in the top frame of Figure 1, with the early-time crater excavation in the bottom frame.

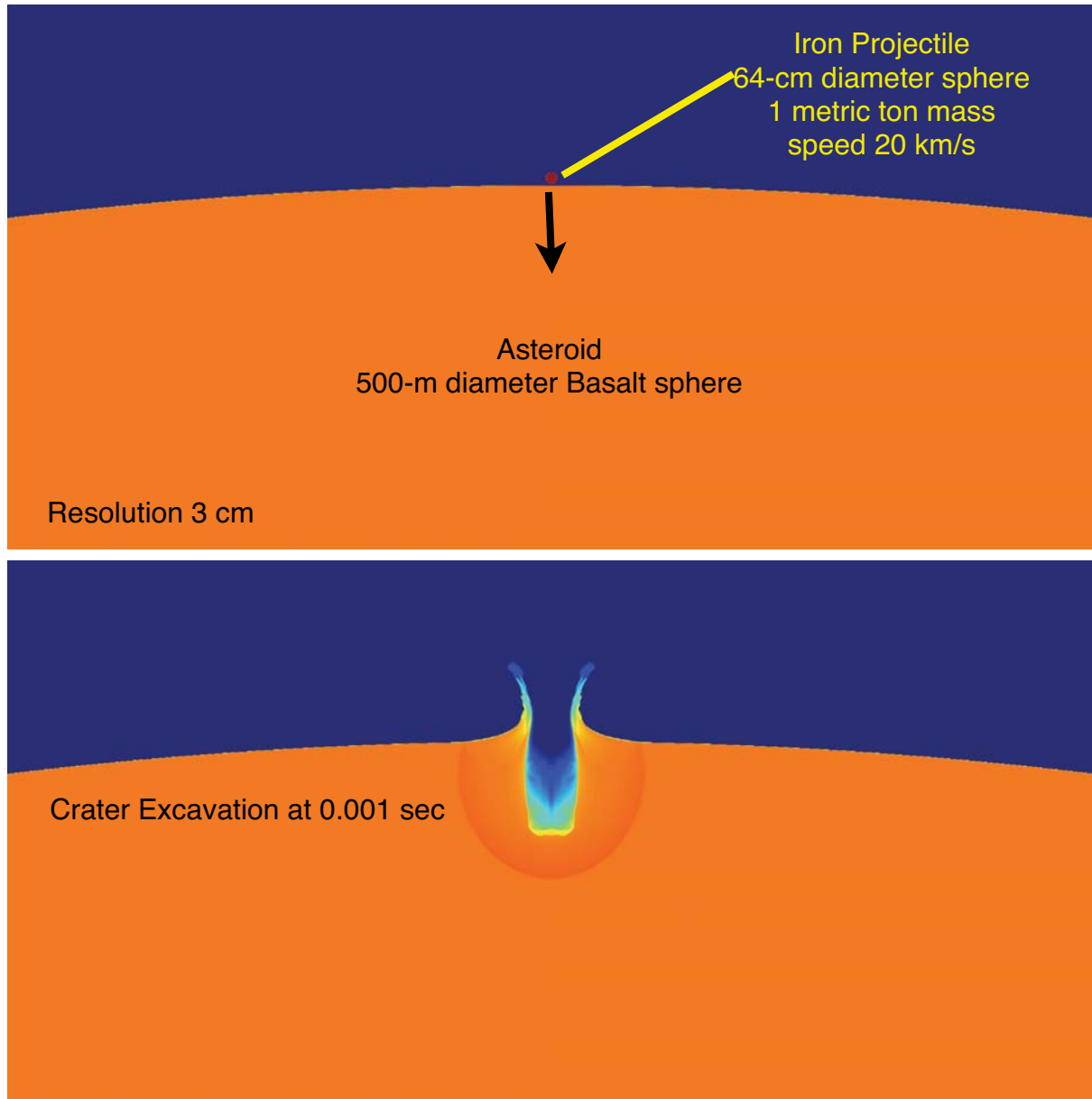


Figure 1. Initial configuration (top) and early-time excavation (bottom) from a kinetic impactor run. An iron spherical projectile of 1 metric ton mass impacts a spherical basalt asteroid at 20 km/s.

After 0.1 second, the crater has opened up and a substantial curtain of ejecta has accelerated backward along the original projectile direction. This is illustrated in Figure 2. The backward-propagating ejecta enhances the momentum delivered to the asteroid, contributing to the  $\beta$  factor.

**Use of tracer particles.** The momentum received by the asteroid is amplified over the initial projectile momentum by the effects of ablation and spall. For simplicity, we consider a spherical asteroid and on-axis impacts only. The projectile arrives from the  $+z$  direction with  $-z$  velocity. For bookkeeping purposes, mass ejected from the asteroid in the  $+z$  direction we consider *ablated*, while mass ejected from the  $-z$  direction we consider *spalled*. The calculation of mass lost to ablation and to spall is done with the aid of Lagrangian tracer particles, placed uniformly throughout the

asteroid body and tracked throughout the calculation. Although self-gravity is not included in the calculation, we consider a tracer and the mass it represents to be lost whenever its outward directed velocity exceeds the computed escape velocity from the asteroid.

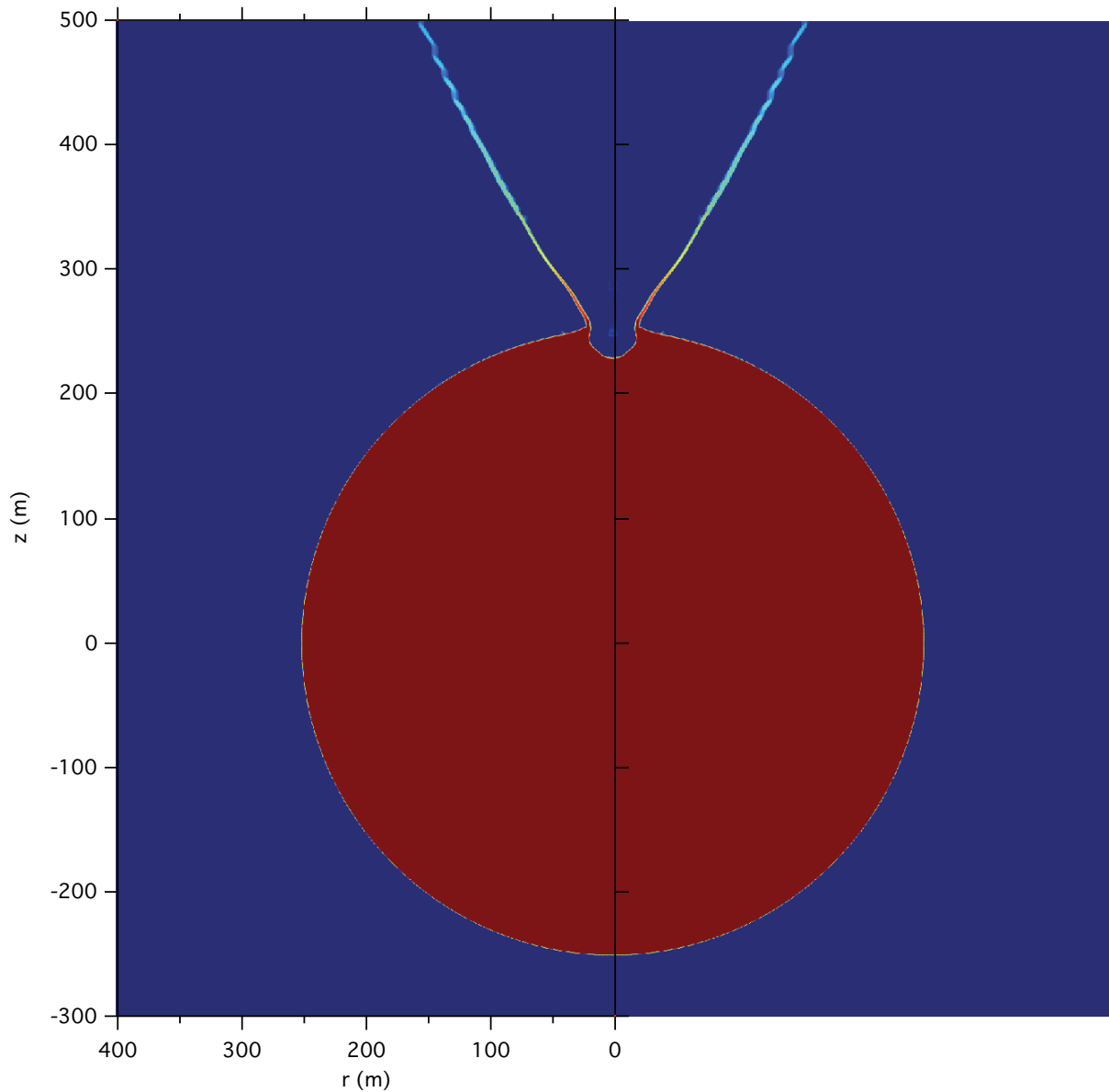


Figure 2. Logarithmic density plot at 0.1 second after the kinetic impact illustrated in Figure 1. The low-density ejecta curtain spreading upward in a cone about the axis enhances the momentum delivered to the asteroid.

The plot in Figure 3 shows initial and final (after 20 seconds) tracer particle positions for one of our calculations. Particles with X superimposed are considered escaped, those with positive velocities ablated, and those with negative velocities spalled. The escape velocity from this asteroid is 20.5 cm/s.

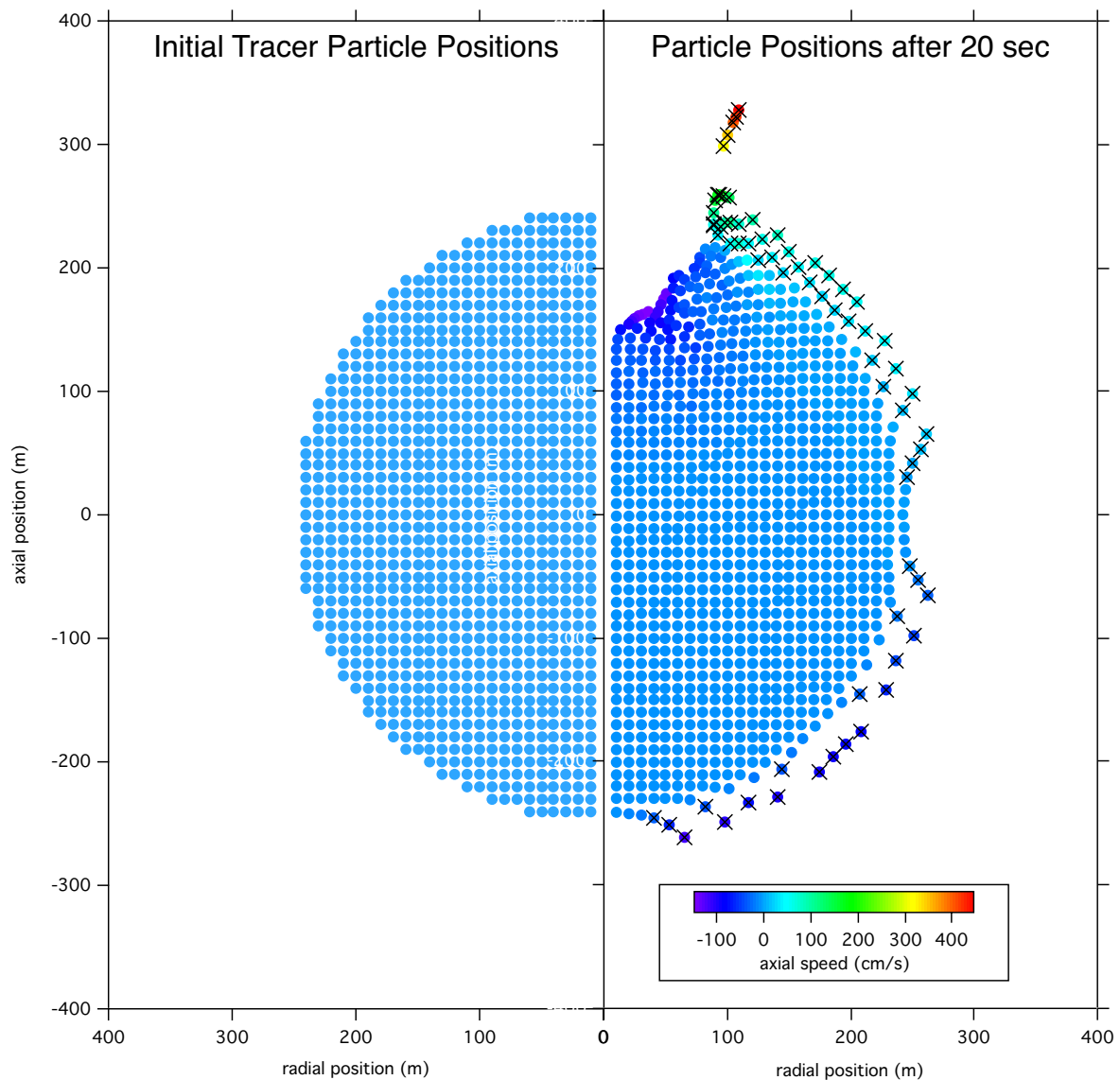


Figure 3. Tracer particle positions and z-velocities at start (left) and end (right) of a kinetic-impact calculation. Lagrangian tracer particles, 946 in number, are placed throughout the volume of the asteroid and tracked throughout the calculation. Those with outward-directed velocities at the end of the calculation greater than the computed escape velocity are marked with a superposed X.

In the left frame of Figure 4, the axial momentum summed over tracers is plotted as a function of time, with separate lines for ablated, spalled, remaining, and all tracers. Ablation starts within a few milliseconds of impact, while spall doesn't occur until the shock wave has passed all the way through the asteroid. In the case plotted here, the contribution of spall is insignificant. The summed momentum of tracers that remain with the asteroid (blue line) is effectively the reflection of the momentum of ablated and spalled tracers. The initial projectile momentum,  $2.15 \times 10^{12}$  g cm/s, is shown as a thin black line with crosses. The momentum delivered to all tracers (red line) does not significantly exceed this.

The effective momentum amplification factor,  $\beta$ , rises dramatically as a function of time due to the effect of front-side ablation from the impact crater. In the cases when spall is significant, it would then be somewhat reduced. Because material continues to boil off the front-side crater,  $\beta$  can continue rising for some time, until the crater cools. Measuring  $\beta$  for a given run can therefore be somewhat arbitrary. For purposes of comparison, we have elected to collect  $\beta$  for all our runs at a uniform time of 0.2 seconds after impact.

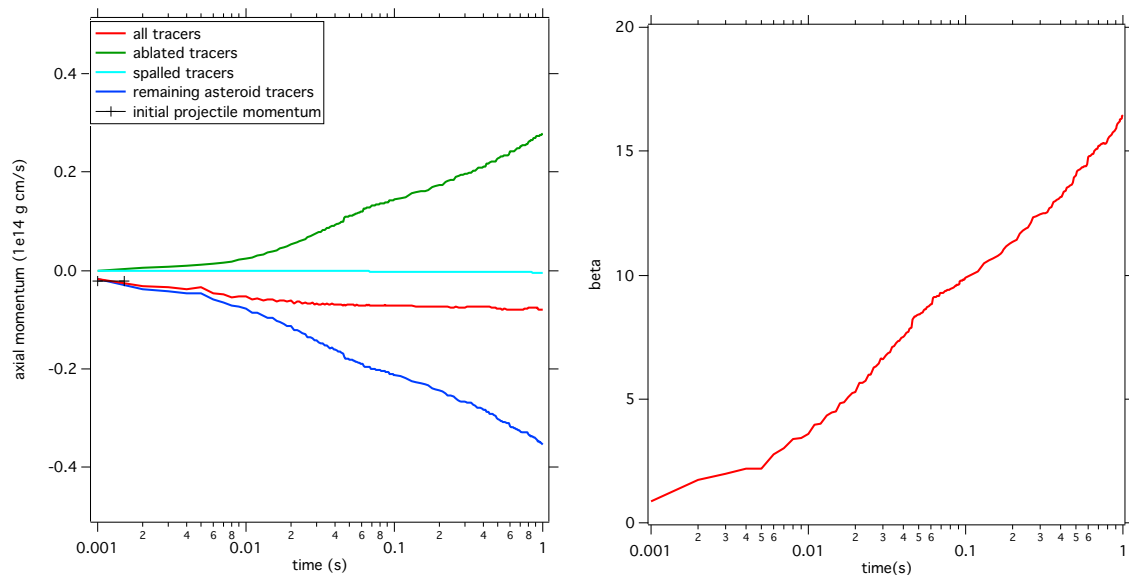


Figure 4. Left frame, axial momentum as a function of time summed over all tracer particles for all tracers (red line), ablated tracers (green line), spalled tracers (cyan line) and remaining tracers (blue line). Right frame, momentum enhancement factor  $\beta$  as defined by equation 1 as a function of time. These plots are from run r1B4 of Table 1, of a 1-metric-ton iron projectile impacting onto a 100-m asteroid of porosity 0.17 at 20 km/s. The collected value of  $\beta$  at 0.2 seconds, is 11.32.

### The effect of porosity.

We find that the momentum amplification factor,  $\beta$ , is substantially reduced by the effects of porosity. This is shown in Figure 5 (right frame) and Table 1, for  $\beta$  collected at the uniform time of 0.2 seconds for all runs. Push velocities, varying from 0.04 cm/s for the 500-m diameter target to 28 cm/s for the 100-m diameter target, are displayed in the left frame of Figure 5. For clarity, only runs using aluminum projectiles are shown in Figure 5, while results for both aluminum and iron projectiles, are included in Table 1. Since asteroids are expected to have porosities of 40% and more, our calculations predict values of 3-5 for  $\beta$ , for dry weak basaltic or alluvial composition. The presence of volatiles could increase  $\beta$  substantially.

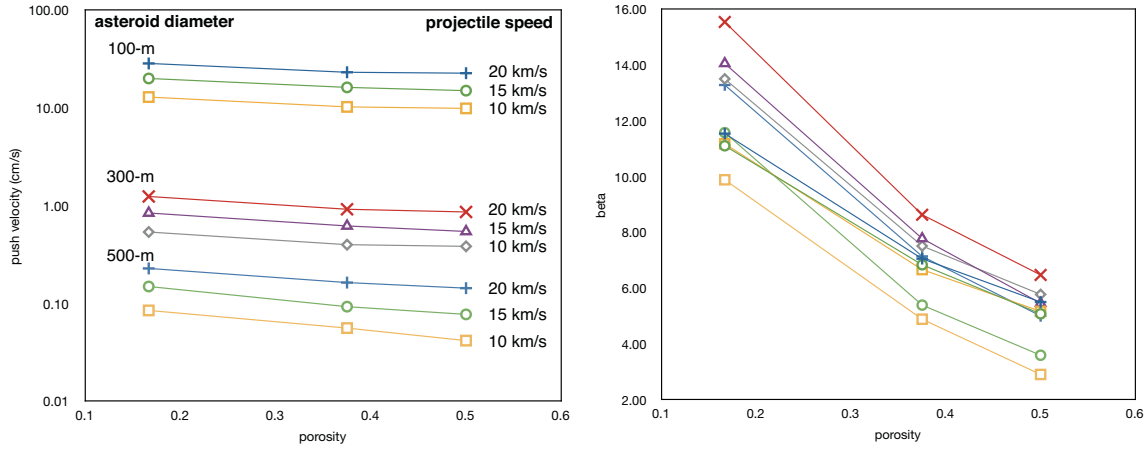


Figure 5. Left frame, expected push velocities for the impact of a one-metric-ton aluminum projectile onto asteroids of the indicated diameter at the indicated velocities, as a function of asteroid porosity. Right frame, values of the momentum enhancement factor  $\beta$  collected at the uniform time of 0.2 seconds for all runs. The symbols and line colors in the right frame correspond to those in the left frame. The sensitivity of  $\beta$  to porosity is very strong. The runs with an iron projectile of the same mass give similar results (see Table 1).

The reason for the reduction of  $\beta$  with porosity is illustrated in Figure 6. The shock wave produced on impact is strongly attenuated through the crushing out of pore space within the rock. This essentially eliminates the possibility of spall from the back and sides of the asteroid in the cases with nonzero porosity, but also strongly reduces the amount and strength of front-side ejecta. The latter, of course, is responsible for the reduction of the momentum enhancement factor  $\beta$ .

Table 1. Table of results from 54 kinetic impact runs

asteroid diameter (m)	projectile speed (km/s)	porosity	aluminum projectile runs					iron projectile runs				
			run name	mass lost to ablation	mass lost to spall	push velocity (cm/s)	beta	run name	mass lost to ablation	mass lost to spall	push velocity (cm/s)	beta
100	20	0.17	q1B4	6.5%	6.8%	28.72	11.6	r1B4	6.9%	6.8%	27.69	11.3
100	20	0.38	q1B6	6.6%	6.2%	23.32	7.1	r1B6	6.6%	6.7%	21.68	6.7
100	20	0.50	q1B8	6.6%	6.6%	22.83	5.5	r1B8	6.2%	6.6%	19.87	4.9
100	15	0.17	q1C4	6.6%	4.2%	20.16	11.1	r1C4	6.6%	5.5%	19.93	11.1
100	15	0.38	q1C6	6.6%	3.0%	16.34	6.8	r1C6	6.2%	3.0%	14.90	6.4
100	15	0.50	q1C8	6.3%	3.0%	15.13	5.1	r1C8	6.5%	2.8%	14.20	4.9
100	10	0.17	q1D4	6.5%	0.7%	13.01	11.2	r1D4	6.3%	0.9%	12.80	11.3
100	10	0.38	q1D6	6.8%	0.2%	10.32	6.7	r1D6	6.5%	0.5%	9.84	6.5
100	10	0.50	q1D8	6.3%	0.2%	9.96	5.2	r1D8	6.8%	0.9%	9.59	5.0
300	20	0.17	q3B4	0.7%	-	1.25	15.6	r3B4	0.7%	-	1.23	15.6
300	20	0.38	q3B6	0.6%	-	0.93	8.6	r3B6	0.6%	-	0.88	8.4
300	20	0.50	q3B8	0.6%	-	0.87	6.5	r3B8	0.6%	-	0.81	6.2
300	15	0.17	q3C4	0.6%	-	0.85	14.1	r3C4	0.6%	-	0.86	14.6
300	15	0.38	q3C6	0.4%	-	0.62	7.8	r3C6	0.4%	-	0.59	7.5
300	15	0.50	q3C8	0.4%	-	0.55	5.5	r3C8	0.4%	-	0.52	5.3
300	10	0.17	q3D4	0.3%	-	0.54	13.5	r3D4	0.3%	-	0.54	13.7
300	10	0.38	q3D6	0.3%	-	0.40	7.5	r3D6	0.3%	-	0.38	7.3
300	10	0.50	q3D8	0.3%	-	0.39	5.8	r3D8	0.3%	-	0.36	5.5
500	20	0.17	q5B4	0.14%	-	0.23	13.3	r5B4	0.14%	-	0.23	13.7
500	20	0.38	q5B6	0.09%	-	0.16	7.2	r5B6	0.09%	-	0.14	6.3
500	20	0.50	q5B8	0.09%	-	0.14	5.0	r5B8	0.09%	-	0.16	5.6
500	15	0.17	q5C4	0.09%	-	0.15	11.6	r5C4	0.09%	-	0.15	11.8
500	15	0.38	q5C6	0.09%	-	0.09	5.4	r5C6	0.09%	-	0.10	5.8
500	15	0.50	q5C8	0.05%	-	0.08	3.6	r5C8	0.05%	-	0.07	3.1
500	10	0.17	q5D4	0.05%	-	0.09	9.9	r5D4	0.05%	-	0.08	10.0
500	10	0.38	q5D6	0.05%	-	0.06	4.9	r5D6	0.05%	-	0.06	4.9
500	10	0.50	q5D8	0.05%	-	0.04	2.9	r5D8	0.05%	-	0.05	3.2

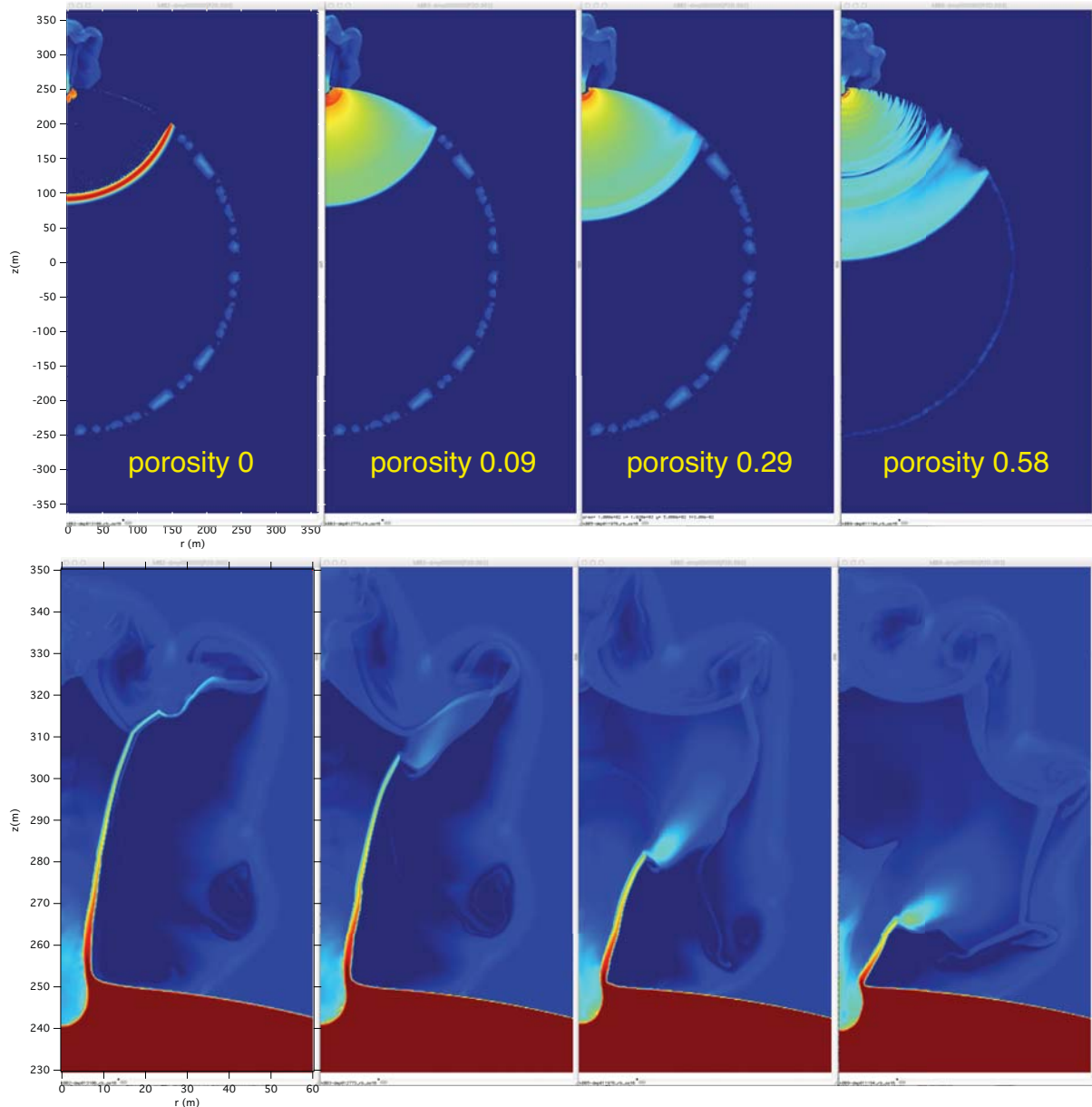


Figure 6. Top, pressure plots at 0.03 seconds after impact, with the pressure in logarithmic scale from 100 to  $1 \times 10^9$  dyn/cm<sup>2</sup> for four different kinetic impact runs (iron impactor at 20 km/s, basalt asteroid) with the indicated asteroid porosities. Bottom, density plots in logarithmic scale from  $1 \times 10^{-7}$  to 1 g/cm<sup>3</sup> for the same four runs at the same time.

## 2. Nuclear Standoff Burst

**Scenario:** The nuclear standoff burst is most likely to be used for an asteroid whose competence is unknown, or if the time between decision and predicted impact is limited. A spacecraft with a nuclear device is sent to intercept, and is fused so as to ignite in an optimal alignment at an optimum burst height. X-radiation and neutrons impinge upon the asteroid, heating the nearest surface and creating a crater, from which material is ejected. As in the kinetic impact case, the momentum given to the asteroid is enhanced over the momentum of the deposited radiation by the reaction

force due to the ablated material. Three early snapshots from a stand-off burst are shown in Figure 7.

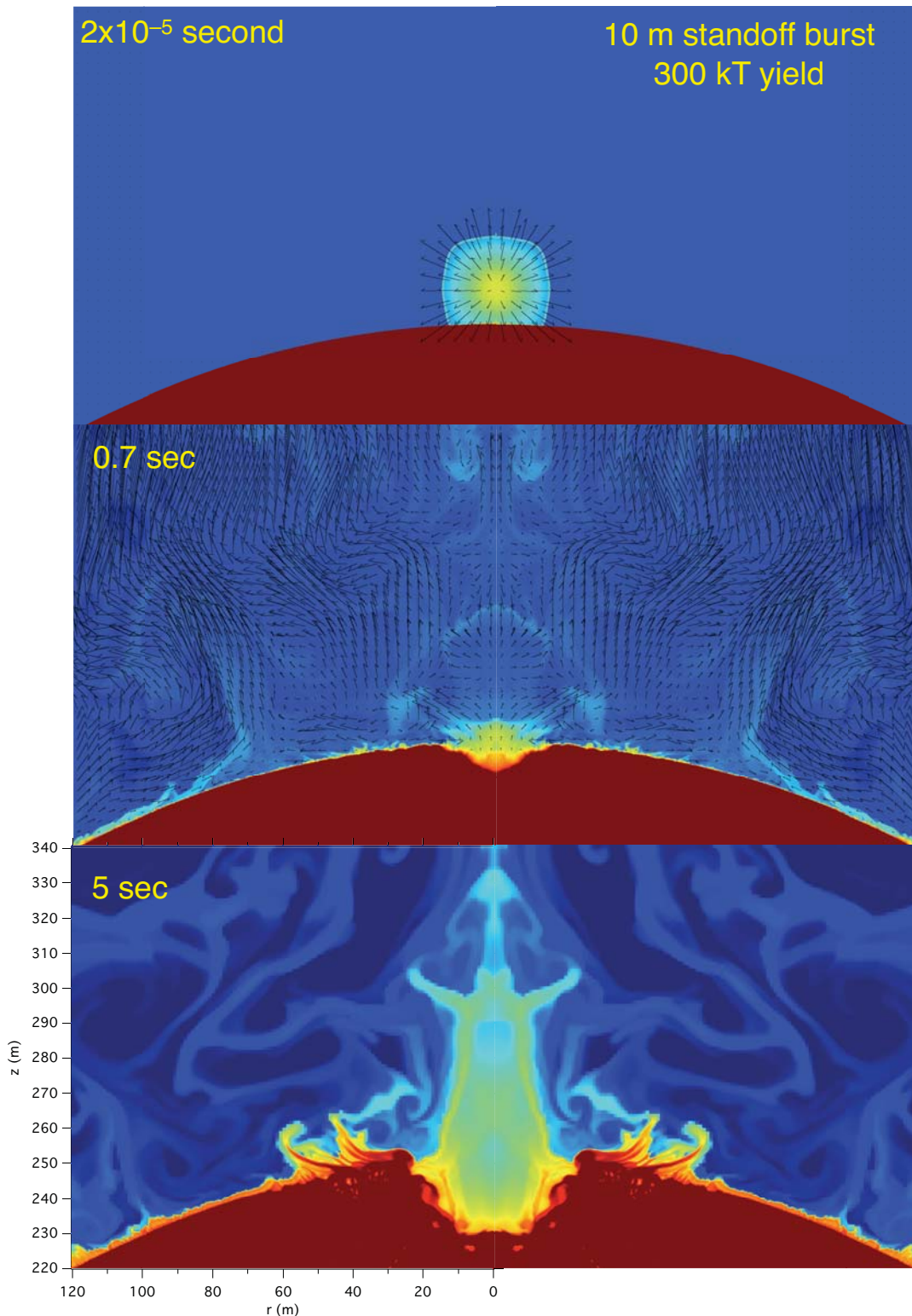


Figure 7. Three snapshots from a stand-off burst calculation. A 300 kT nuclear device is set off 10 m above the surface of a 500-m diameter basaltic asteroid. This results in the production of a crater from which hot material is ablated, producing a thrust that contributes to the asteroid's deflection.

**Optimum height of burst.** Earlier studies have produced conflicting results on the optimum burst height for maximum deflection. The geometrical optimum height of burst found by Ahrens and Harris [4] was 40% of the asteroid diameter. Consideration of radiation penetration depth, efficiency of ablation, and direction of ejecta have led to different estimates over the years, some closer to the asteroid, some farther away.

With the RAGE hydrocode, we have performed a series of simulations of bursts of different energies at different heights over a 500m diameter asteroid of solid basalt, using the LANL SESAME equation of state and opacity tables. We find that closer bursts, right down to the asteroid surface give stronger net pushes, but if the burst is too close, the asteroid is increasingly likely to be disrupted.

The degree of disruption depends very strongly on the material properties of the asteroid and demands better strength models, equations of state for asteroid materials, and knowledge of the porosity of the asteroid.

Closer bursts are more efficient at delivering momentum to the asteroid, while also increasing the potential for its disruption. Table 2 lists results for standoff bursts with 3 different yields at varying distances from a 500 m diameter solid (nonporous) asteroid, with an equation of state of alluvium or basalt. The columns marked “degree of disruption” gives the ratio of total radial momentum to axial momentum imparted to the tracer particles. Although these runs were not long enough to show disruption, a larger number makes disruption more likely. In Figure 8 are displayed the axial push velocity and degree of disruption as functions of burst height.

Table 2. Results from 29 height-of-burst nuclear standoff runs

porosity	yield (kT)	height of burst (m)	run name	alluvium EOS				basalt EOS				
				mass lost to ablation	mass lost to spall	push velocity (cm/s)	degree of disruption	run name	mass lost to ablation	mass lost to spall	push velocity (cm/s)	degree of disruption
0.00	300	60	hJP6	-	-	0.06	0.48	hIP6	-	-	0.06	0.30
0.00	300	40	hJQ6	-	-	0.09	0.46	hIQ6	-	-	0.07	0.40
0.00	300	25	hJR6	-	-	0.07	0.72	hIR6	-	-	0.05	0.80
0.00	300	15	hJS6	0.05%	-	0.07	1.12	hIS6	0.05%	-	0.04	2.27
0.00	300	10	hJT6	0.10%	-	0.10	1.22	hIT6	0.10%	-	0.14	1.17
0.00	300	5						hIU6	0.61%	1.62%	0.18	1.63
0.00	600	100	hJO7	-	-	0.09	0.38	hIO7	-	-	0.06	0.30
0.00	600	60	hJP7	-	-	0.11	0.65	hIP7	-	-	0.07	0.53
0.00	600	40	hJQ7	-	-	0.15	0.64	hIQ7	-	-	0.08	0.71
0.00	600	25	hJR7	-	-	0.15	0.67	hIR7	-	-	0.09	0.94
0.00	600	15	hJS7	0.10%	0.06%	0.16	0.93	hIS7	0.10%	-	0.10	1.46
0.00	600	10	hJT7	0.29%	0.15%	0.16	1.38	hIT7	0.29%	0.15%	0.19	1.18
0.00	600	5	hJU7	2.02%	2.18%	0.17	2.25	hIU7	2.02%	2.27%	0.24	1.77
0.00	1200	100	hJO8	-	-	0.15	0.53	hIO8	-	-	0.11	0.36
0.00	1200	60	hJP8	-	0.06%	0.22	0.74	hIP8	-	-	0.12	0.72
0.00	1200	40	hJQ8	-	0.11%	0.25	0.78	hIQ8	-	-	0.15	0.84
0.00	1200	25	hJR8	-	0.11%	0.27	0.76	hIR8	-	-	0.16	1.04
0.00	1200	15	hJS8	0.19%	0.23%	0.29	0.95	hIS8	0.19%	0.23%	0.18	1.39
0.00	1200	10	hJT8	0.60%	1.36%	0.12	3.02	hIT8	0.60%	1.36%	0.19	2.10
0.00	1200	5	hJU8	7.62%	3.63%	1.45	0.41	hIU8	7.62%	3.63%	0.85	0.77

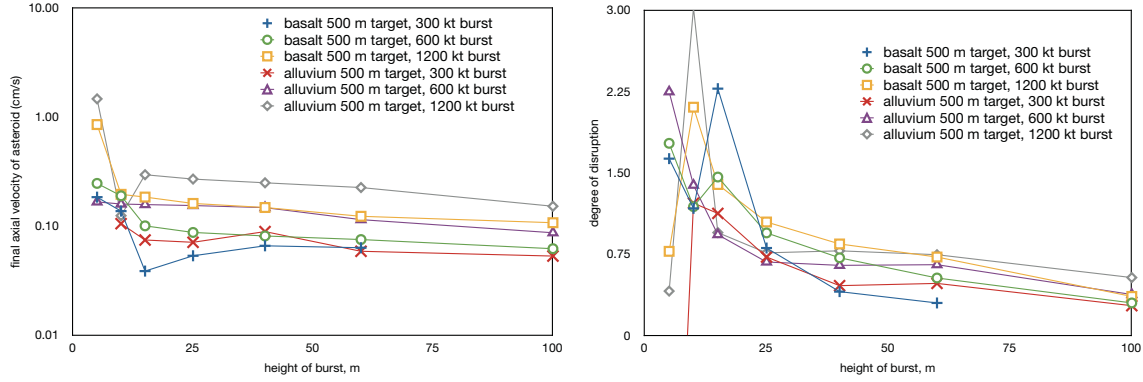


Figure 8. Left, axial push velocity as a function of burst height for a nuclear stand-off burst of the indicated yield, for a 500-m diameter asteroid with alluvium or basalt equation of state. Right, degree of disruption, as computed from the ratio of imparted radial to axial momentum to the tracer particles. Closer bursts give greater pushes, as expected, but also increase the likelihood of disruption.

**Calculating  $\beta$  for a standoff burst.** As in the kinetic impact case, it is desired to formulate a figure of merit for the efficiency of momentum delivery to the asteroid. We use the same symbol for the momentum multiplication factor,  $\beta$ , now taken to be the ratio of the asteroid momentum after the burst event ( $p_{\text{push}}$ ) to the momentum deposited by radiation from the nuclear device. This latter quantity is estimated as the energy of the device yield ( $E_{\text{burst}}$ ), divided by the speed of light and multiplied by the fractional solid angle ( $\omega/4\pi$ ) subtended by the asteroid from the burst position:

$$\beta_{\text{standoff}} = \frac{P_{\text{push}}}{E_{\text{burst}} \frac{\omega}{c \ 4\pi}} \quad (2)$$

As in the kinetic impact case, porosity affects the efficiency of momentum enhancement in the standoff burst case, although the effect is not as strong. Table 3 lists results for a burst yield of 300 kT at a standoff of 10 meters from a 500 m diameter asteroid.

Table 3. Results from 14 nuclear-standoff runs with varying asteroid porosity

porosity	yield (kT)	height of burst (m)	run name	alluvium EOS			beta	run name	basalt EOS			beta
				mass lost to ablation	mass lost to spall	push velocity (cm/s)			mass lost to ablation	mass lost to spall	push velocity (cm/s)	
0.00	300	10	hCB2	0.05%	0.06%	0.08	3.57	hBB2	0.10%	-	0.09	5.13
0.09	300	10	hCB3	0.05%	-	0.06	2.44	hBB3	0.02%	-	0.05	2.60
0.17	300	10	hCB4	0.03%	-	0.07	2.74	hBB4	0.02%	-	0.04	1.80
0.29	300	10	hCB5	0.05%	-	0.07	2.37	hBB5	0.07%	-	0.06	2.19
0.38	300	10	hCB6	0.06%	-	0.08	2.42	hBB6	0.02%	-	0.01	0.29
0.44	300	10	hCB7	0.03%	-	0.11	2.71	hBB7	0.09%	-	0.06	2.00
0.50	300	10	hCB8	0.06%	-	0.13	2.98	hBB8	0.07%	-	0.10	2.72

The results are somewhat inconsistent with expectations, which may indicate that equation (2) does not give a good estimate of the effective momentum enhancement factor.

### **3. Conclusions**

The kinetic impact and nuclear stand-off burst are two of the best available options for asteroid deflection, if the need should arise. For small and competent asteroids, kinetic impact is surprisingly effective, and would be even more effective for volatile-rich bodies. For larger and less competent bodies, the nuclear option is the best available, particularly if warning times are short.

#### **References:**

- [1] Barbee, B.W. et al. (2013) Planetary Defense Conference IAA-PDC13-04-07.
- [2] Housen, K.R. & Holsapple, K.A. (2012) Lunar and Planetary Science Conference, paper 2539.
- [3] Gittings, M. et al., Computational Science and Discovery, 1, 015005.
- [4] Ahrens, T.J. & Harris, A.W. (1994) in Hazards due to Comets and Asteroids.